32. Fachtagung "Experimentelle Strömungsmechanik"
9.- 11. September 2025, Darmstadt

Geschwindigkeitsmessungen in einem offenen rechteckigen Kanal - Vergleich zwischen 2D2C-PIV und akustischen Ultraschall Doppler Profil Sensor (ADCP) Daten

Velocity measurements in an open rectangular channel – Comparison between 2D2C-PIV and acoustic Doppler profiler (ADCP) data

Mohammd Tanvir Haque Tuhin[2,3], Marc Ladwig[1], Daniel P. Gradzki[1], Ralph Lindken[1], Christoph Mudersbach[2], Reinhard Hinkelmann[3]
[1]Institut für Thermo- und Fluiddynamik, Fachbereich Mechatronik und Maschinenbau, Hochschule Bochum, Am Hochschulcampus 1, 44801 Bochum
[2]Lehr- und Forschungsgebiet Wasserbau und Hydromechanik, Fachbereich Bau- und Umweltingenieurwesen, Hochschule Bochum, Am Hochschulcampus 1, 44801 Bochum
[3]Fachgebiet Wasserwirtschaft und Hydrosystemmodellierung, Technische Universität Berlin, Gustav-Meyer-Allee 25, 13355 Berlin

2D2C-PIV, turbulente offene Kanalströmung, Ultraschall-Doppler-Profil-Strömungsmesser (ADCP)
2D2C-PIV, turbulent open-channel flow, Acoustic Doppler Current Profiler (ADCP)

Zusammenfassung

Akustische Doppler-Strömungs-Profilsensoren (ADCPs) werden in der Gerinnehydraulik häufig für Geschwindigkeits- und Abflussmessungen eingesetzt, da sie auch in sedimentbeladenen und optisch schwierigen Umgebungen eine zuverlässige Datenerfassung ermöglichen. Ihre Messfähigkeit kann jedoch durch Faktoren wie akustische Interferenzen, lokalen Strömungsbedingungen (Turbulenz, Gradienten) sowie, außerhalb bestimmter Grenzwerte bezogen auf Größe und Konzentration der Schwebstoffe, negativ beeinflusst werden, wodurch die Messqualität insgesamt beeinträchtigt werden kann. Zudem kann das ADCP von Labormessungen in Gerinneströmungen bis hin zu Feldversuchen in Freigewässern eingesetzt werden. Im Gegensatz dazu bieten optische Verfahren wie die Particle Image Velocimetry (PIV) eine höhere räumliche Auflösung und detailliertere Einblicke in Strömungsstrukturen, insbesondere unter kontrollierten Laborbedingungen. Sie erfordern jedoch einen optischen Zugang, wodurch der Einsatz im Feld i.d.R. weniger praktikabel ist. Zur Bewertung beider Systeme unter identischen Bedingungen führten wir eine vergleichende Messkampagne mit simultanen ADCP- und 2D2C-PIV-Messungen in einem offenen Wasserkanal im Labormaßstab durch.
In diesem Beitrag präsentieren wir Messergebnisse, die in einem 16 m langen offenen Kanal mit rechteckigem Querschnitt von 0,6 x 0,56 m Wasserhöhe im Labor für Wasserbau und Hydromechanik an der Hochschule Bochum erhoben wurden. Die Messreihen umfassten Reynolds-Zahlen im Bereich von $Re = 6{,}48 \cdot 10^4$ bis $1{,}76 \cdot 10^5$ sowie Froude-Zahlen zwischen $Fr = 0{,}049$ und $0{,}134$. Die 2D2C-PIV und ADCP - Messungen wurden zunächst unter

Klarwasserbedingungen durchgeführt, wobei Geschwindigkeitsprofile im vollständig entwickelten turbulenten Strömungsbereich erfasst wurden. Unsere Experimente ermöglichen einen direkten Vergleich von mittleren Geschwindigkeiten und Turbulenzgrößen zwischen beiden Systemen.

Abstract

Acoustic Doppler Current Profilers (ADCPs) are widely used in open-channel hydraulics for velocity and discharge measurements, offering robust data collection even in sediment-laden and optically challenging environments. However, their performance can be affected negatively by factors such as acoustic frequency, local flow conditions (turbulence, gradients), and beyond certain thresholds, the size and concentration of suspended particles, which influence measurement quality. In addition, the ADCP can be used from laboratory measurements in laboratory channel flows to field tests in open waters. In contrast, optical techniques like Particle Image Velocimetry (PIV) provide higher spatial and temporal resolution and detailed insight into flow structures, particularly in controlled laboratory settings, but required optical access, which usually limits their practicability concerning open field measurements. To evaluate both systems under identical conditions, we conducted a comparative study using simultaneous ADCP and 2D2C-PIV measurements in a laboratory open water channel.

In this contribution, we present results from measurements conducted in a 16 m open-channel flume with a rectangular cross-section of 0,6 m x 0,56 m water height at the Laboratory for Hydraulic Engineering and Hydromechanics at Bochum University of Applied Sciences. The experiments covered Reynolds numbers between $Re = 6.48 \cdot 10^4$ and $1.76 \cdot 10^5$ and Froude numbers between $Fr = 0.049$ and 0.134. The 2D2C-PIV and ADCP measurements were initially performed under clear-water conditions, capturing velocity profiles in the fully developed turbulent flow region. Our experiments allow for a direct comparison of mean velocities and turbulence quantities between both systems.

1 Introduction

Understanding the flow dynamics in open-channel flows is crucial for many applications in hydraulic engineering and experimental fluid mechanics, including river engineering and sediment transport (Chow 1959, Nezu and Nakagawa 1993, Chanson 2004). In particular, laboratory experiments provide controlled environments to investigate these flows and, e.g., to calibrate numerical models, where accurate velocity measurements are essential for validating theoretical predictions and model improvements. Established intrusive measurement techniques like electromagnetic current meters and Pitot tubes can disrupt the flow and offer limited spatial data, driving the shift toward non-intrusive systems like acoustic (e.g., ADCP), optical (e.g., PIV), ultrasound, and radar-based sensors that measure flow without physically contacting the fluid (Nones et al. 2022).

ADCP sensors measure flow velocities by leveraging the Doppler shift of acoustic signals reflected by suspended particles, enabling velocity profile measurement of flow structures. Recent advancements, including broadband and pulse-coherent systems, have enhanced their accuracy (Simpson 2001). Though mainly used for discharge measurements, e.g. the integral volumetric flux, emerging studies show that integrating ADCP data with machine learning techniques can substantially enhance hydrodynamic analyses and sediment transport prediction (Tuhin and Mudersbach 2025). Several studies have explored the capabilities and limitations of ADCP and PIV systems separately. Some studies (Nystrom et al. 2002; Nystrom et al. 2007; Mueller et al. 2007) highlighted that while ADCP sensors perform well for mean flow characterization, they face challenges in accurately resolving near-boundary velocities and turbulence structures due to spatial averaging and Doppler noise. These findings underscore the

GALA e.V., Karlsruhe, Germany, ISBN 978-3-9827594-0-1

need for complementary spatially higher resolved velocity data as it is achievable with optical techniques like PIV, particularly in the near-wall ground region. Direct comparisons of these techniques in controlled laboratory settings are notably limited. While several studies have examined the accuracy of ADCP measurements relative to point-based techniques such as Acoustic Doppler Velocimeters (ADV) (Nystrom et al. 2007, Kim and Kang 2011, Muste et al. 2010), laboratory-based evaluations against spatially resolved PIV data or other optical methods remain sparse. This gap is particularly important to be addressed, as understanding the differences in measurement capabilities and potential sources of error between ADCP and PIV systems is essential for advancing the accuracy of flow measurements in laboratory experiments and for further transfer into open-field measurements as used for discharge estimates.

2 Experimental setup

2.1 Open channel facility

ADCP and 2D2C-PIV measurements were accomplished in a 16 m long open water channel with a rectangular cross-section of 0.6 m width and 0.8 m height. The recirculatory flow is driven by three centrifugal pumps with a maximum flow rate of 400 m³/h. The volumetric flux was additionally measured with a magnetic inductive flow meter (Promag 10W1F, E+H) pertaining a maximum relative error of ± 0.14 % of the momentary flow rate. The open channel entrance section consists of an upstream located settling chamber with a subsequent turbulence screen with a rectangular mesh of 30 mm cell spacing. To ensure controllable inflow conditions, an integrated float plate attenuates additional pulsations of the vertical convective flow in the settling chamber, which nevertheless yields remaining surface waves in the downstream channel with flow rate dependent wave amplitudes. Pure tap water is used at ambient conditions in the temperature range between 19.5 – 21.8 °C. The vertical channel walls are made of soda-lime float glass segments with 12 mm thickness, embedded in a horizontal bed of polished stainless steel. All measurements presented here were acquired 8.5 m downstream the entrance section of the flume and preliminary test measurements showed that the flow was fully developed at this point. The coordinate system is shown in Fig. 1 and Fig. 2 with x-axis along streamwise and y-axis in spanwise vertical direction, located in the flume center plane at z = 0.

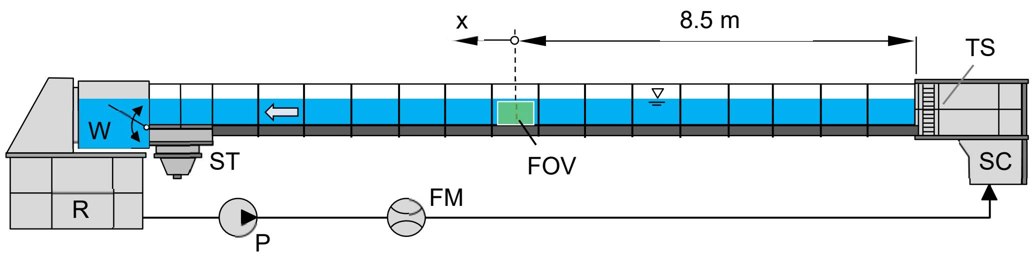

Figure 1: Schematic overview of the open water channel at the Laboratory for Hydraulic Engineering and Hydromechanics at Bochum University of Applied Sciences. Settling chamber (SC) with turbulence screens (TS), field of view (FOV) located at 8.5 m downstream the entrance section, circulation pump (P), magnetic flow meter (FM), height-adjustable weir (W), water reservoir (R) and sediment trap (ST). Flow direction within the open channel test-section is from right to left.

All measurements were done at a constant water level height of H = 0.56 m and flow rates between 140 m^3/h to 380 m^3/h leading to corresponding Reynolds numbers, based on the mean velocity and water level, between $Re = 6.48 \cdot 10^4$ and $1.76 \cdot 10^5$. The horizontal channel inclination was set to $0° \pm 0.002°$. The most relevant experimental parameters are listed in Table 1.

GALA e.V., Karlsruhe, Germany, ISBN 978-3-9827594-0-1

Table 1: Experimental parameters

case			C 1	C 2	C 3	C 4	C 5	C 6
flow rate	Q	m³/h	140 ± 0.64	180 ± 0.84	200 ± 1.14	320 ± 1.74	340 ± 1.84	380 ± 2.0
mean velocity	U_m	m/s	0.116	0.149	0.165	0.265	0.281	0.314
nominal water height	h	m	0.56	0.56	0.56	0.56	0.56	0.56
kinem. viscosity	ν	m²/s	$9.86 \cdot 10^{-7}$	$10.01 \cdot 10^{-7}$	$10.01 \cdot 10^{-7}$	$9.84 \cdot 10^{-7}$	$9.96 \cdot 10^{-7}$	$9.84 \cdot 10^{-7}$
Reynolds number	Re	-	$6.48 \cdot 10^{4}$	$8.33 \cdot 10^{4}$	$9.26 \cdot 10^{4}$	$1.48 \cdot 10^{5}$	$1.57 \cdot 10^{5}$	$1.76 \cdot 10^{5}$
Froude number	Fr	-	0.049	0.063	0.071	0.113	0.120	0.134

2.2 ADCP measurement setup

ADCP measurements were conducted with a SonTek RS5 ADCP (3 MHz broadband pulse-coherent) in a four-beam Janus arrangement (25° tilt, 3° beam width) plus a vertical depth beam. We used the default profiling device settings (Cell_Start = 0.103 m, Cell_Size = 0.050 m), which produces a series of closely spaced vertically cells with slight overlap (~ 15 %) to ensure seamless coverage without sacrificing acoustic return strength. The ADCP was leveled within ± 1° with respect to the vertical axis and mounted on an adjustable aluminum frame at the channel center-plane, 8.5 m downstream of the entrance section. After each discharge has stabilized, data were acquired for at least 10 minutes in SonTek RSQ (1 Hz ping (sample) rate with 30-ping ensembles resulting in an acquisition time of 30 seconds for a single measurement sample), applying a correlation threshold of 0.3 to secure bottom-locked returns. This setup yields a single-ping precision of ± 0.25 % (≈ 0.5 mm/s), corresponding to an average standard deviation below 0.01 m/s, with continuous sound-speed profiling maintaining a range accuracy throughout.

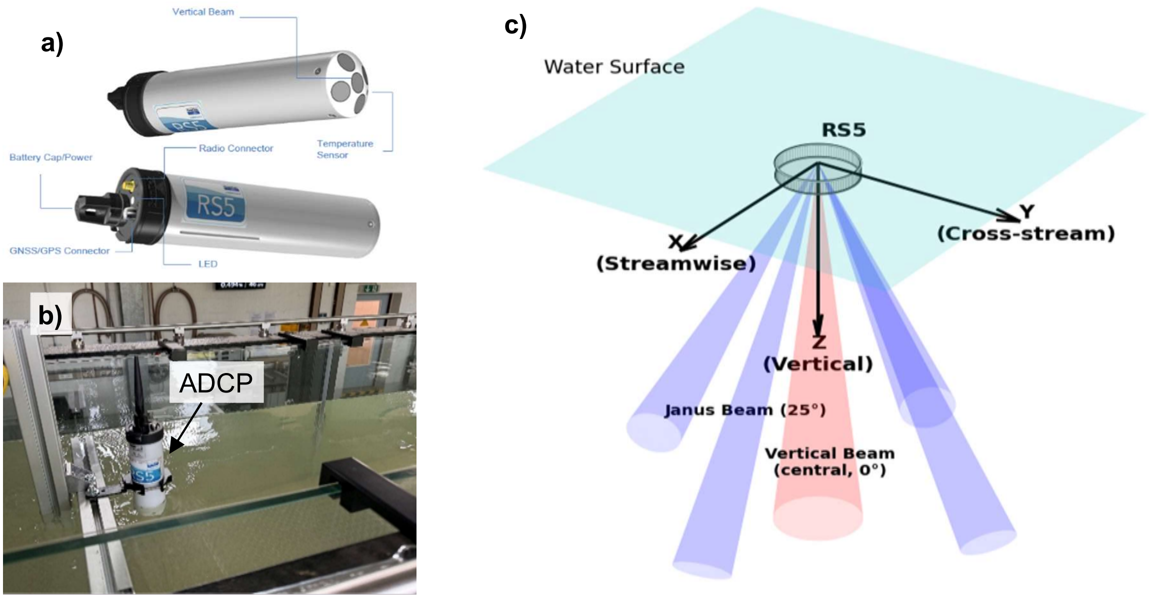

Figure 2: a) Schematic overview of ADCP system, b) experimental arrangement within the open channel, and c) principle of cross-formation of the vertical acoustic beam formation used for velocity data acquisition within the open-channel.

2.3 2D2C-PIV measurement setup

We used a 2D2C-PIV system which consists of a 16-bit CMOS camera (Imager sCMOS, La Vision) with 2550 × 2160 pixels (pixel size 6.5 µm) equipped with a 100 mm macro lens (Zeiss Macro Planar T2,8/100 mm). Illumination was provided by a double-pulse frequency doubled YAG: laser (Quantel Evergreen 200, repetition rate 15 Hz) with a maximum pulse energy of 200 mJ each, at a light wavelength of 532 nm. Pulse energy was attenuated with a dielectric edge filter (Metrolux VAM 532) to about 65 mJ per pulse during recording, guided by a laser guiding arm and a light sheet optic for beam expansion in the channel center-plane. The light sheet thickness was set to ≅ 1.0 mm. Temporal synchronization between recording and laser illumination was provided by an integrated timing unit (LaVision PTU X, temporal jitter < 1 ns). The lens aperture was adjusted to $f\#$ = 2.8. For each flow rate a series of 7.500 double frames were recorded at 15 Hz. The flow is seeded with white spherical polyamide PA12 particles with a density of 1.016 kg/m³ and a mean diameter of d_{50} = 20 µm. The particle time constant is $\tau_P \cong 30$ µs assuming Stokes drag, which leads for the present measurements to a maximum particle Stokes number of $St = \tau_P / \tau_F = 1.4 \cdot 10^{-3}$ with $\tau_F \cong 21.3$ ms being the time scale of small-scale flow structures at highest flow rate. We therefore assume that the particles faithfully follow the flow to a sufficient extent, within the investigated flow regimes. Particles were injected as premixed suspension into the flow 500 mm upstream the turbulence mesh and 9 m upstream the field of view (FOV) (see Fig. 1 and Fig. 3). An iterative optimization of the seeding concentration was done in-situ on double frame recordings to yield a valid detection probability on final recordings with a mean number of minimum 5 valid particle pairs per interrogation window (Keane and Adrian 1992, Adrian and Westerweel 2011). Further PIV related parameters are listed in Table 2.

Table 2: PIV setup parameters

case			C 1	C 2	C 3	C 4	C 5	C 6
flow rate	Q	m³/h	140	180	200	320	340	380
Exposure time delay	Δt	ms	10.8	8.4	7.5	4.7	4.4	4.0
Spatial dynamic range[a]	SDR	-			152			
Dynamic velocity range[a]	DVR	-	316	310	296	253	217	193

[a](Adrian 1997)

The final seeding concentration was 4 g/m³ based on the total amount of circulating fluid in the channel. Geometric calibration within the field of view was done with a two-level calibration plate (LaVision type 106-10) with a pattern of dots with 3 mm diameter and 10 mm spacing. We used a pinhole model for image mapping, yielding to a scaling factor of 8.08 pixel/mm and a maximum calibration fit error of 0.0851 pixel (0.01 mm).

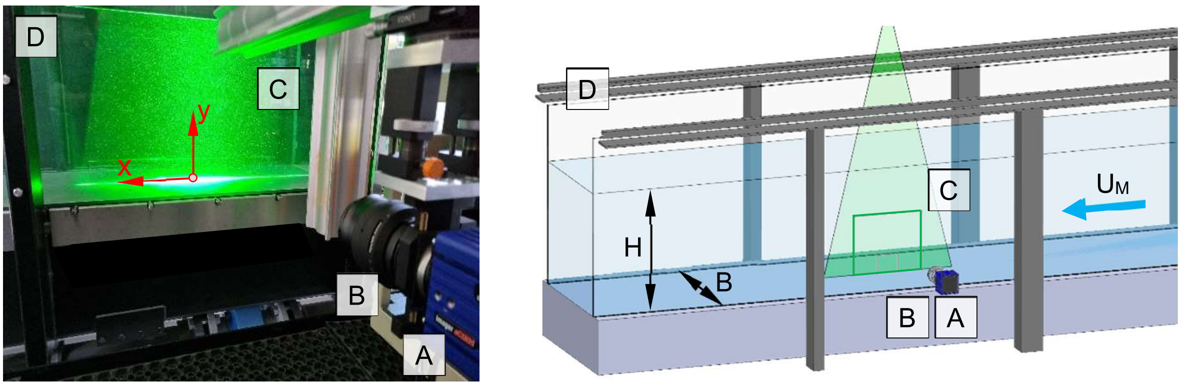

Figure 3: Left: Experimental setup: 2D2C-PIV system within the open water channel flow facility at the Laboratory for Hydraulic Engineering and Hydromechanics at Bochum University of Applied Sciences. (A) camera, (B) lens, (C) field of view (FOV) and (D) open-channel facility.

 ISBN 978-3-9827594-0-1

3 Methodology and data processing

3.1 ADCP sampling and data processing

For the depth-resolved velocity samples acquired with the ADCP sensor, we applied the following streamlined preprocessing workflow as follows:

Each discharge dataset was imported and processed in Python via scipy.io.loadmat to retrieve the WaterTrack velocity array (60 bins × 4 components × 600 - 800 pings) and the associated correlation field (acoustic-return quality across all beams and depth cells). We flagged a ping as valid if any bin - beam correlation exceeded 0.3, then truncated the time series to the continuous block of valid, bottom-locked pings (e.g., pings 19 - 531 at 200 m^3/h). Next, any depth cell whose correlation never rose above 0.3 over that interval was discarded, thereby removing the instrument's blanking zone and unreliable bed echoes and exactly seven valid bins were retained per run. Finally, we converted these bin indices into calibrated depths below the free surface using the known transducer submergence (0.045 m) and cell geometry (Cell_Start and Cell_Size) according to Eq. 1:

$$A = 0.045 + (Cell_{Start} + (i + 0.5)Cell_{size})) \tag{1}$$

Seven depths (≅ 0.1 - 0.47 m) were yielded for all subsequent 2D/3D velocity over depth datasets (see. Fig. 4).

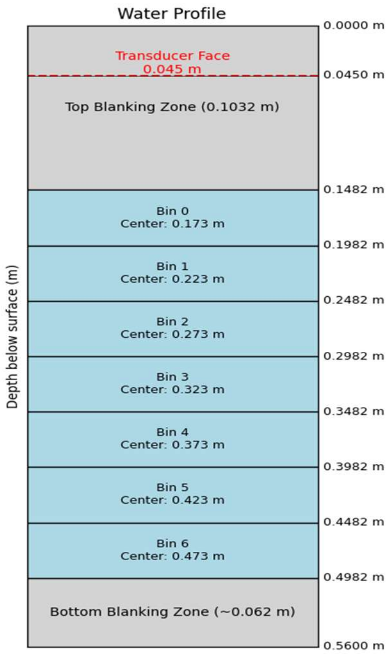

Figure 4: An example of resulting vertical ADCP depth bins for the Re = 6.48 x 10^4 case (Q = 140 m^3/h). Grey shaded blanking zones showing sub-areas without or invalid velocity data by ADCP sensor.

In the next processing step, we combined each 4-component velocity block (bins × 4 × pings) into 2-D and 3-D velocity arrays via Eq. 2:

$$U_{2D} = \sqrt{u^2 + v^2} \quad , \quad U_{3D} = \sqrt{u^2 + v^2 + w^2} \tag{2}$$

The velocity arrays were then reshaped to (bins × 1 × pings), then each run was truncated to the shortest common segment of 515 pings (= samples), yielding uniform 7 × 1 × 515 velocity matrices for all subsequent analyses and profile plots. Finally, these matrices were plotted as mean velocity over depth profiles with bin markers and inverted y-axis.

GALA e.V., Karlsruhe, Germany, ISBN 978-3-9827594-0-1

3.2 2D2C-PIV acquisition and data processing

Single exposed double frames were recorded in the streamwise center plane of the open channel for each flow rate according to Table 1. The exposure time delay was optimized leading to mean particle displacements in streamwise direction of 10 pixels in the sensor plane. The nominal optical magnification was set to M_0 = 0.055 resulting in a field of view of 300 x 269 mm. Image preprocessing was then applied on raw images, first to minimize reflections from the channel bottom surface located at y = 0 and secondly to accommodate intensity fluctuations caused by the unsteady curvature of the free water surface, causing irregular intensity patterns in the focal plane. It first consisted of a subtraction of the sliding intensity minimum for each pixel position and a spatial low-pass filter to effectively eliminate remaining reflections, followed by an intensity normalization and a Gaussian smoothing filter to ensure Gaussian shaped particle intensity distributions. Then cross-correlation was applied on image pairs in multiple passes, starting from an initial interrogation window size of 96 x 96 pixels with 50 % overlap followed by four iterations with a final interrogation window size of 32 x 32 pixels with 50 % overlap, each, resulting in a number of 161 x 135 vectors with a spatial resolution of 1.98 mm between adjacent vectors. We were able to reconstruct vectors down to 1.6 mm above the channel ground surface. An elliptical weighting function (4:1) was applied on the interrogation windows in streamwise (x) direction to account for wall normal velocity gradients. Universal outlier detection with rejection of spurious vectors exceeding a difference to the average of twice the standard deviation of the nearest nine surrounding vectors is used for error analysis (Westerweel and Scarano 2005). A random sample showed that the fraction of valid vectors was predominantly greater than 97 % for all flow rates. In addition, the convergence of the ensemble mean values of velocity and Reynolds stresses was calculated as a ratio to the long-term mean, which is shown in Fig. 5. PIV-based uncertainties of the velocity estimates are computed via the correlation statistics approach within Davis 10 (Wienecke 2015, Sciacchitano and Wienecke 2016).

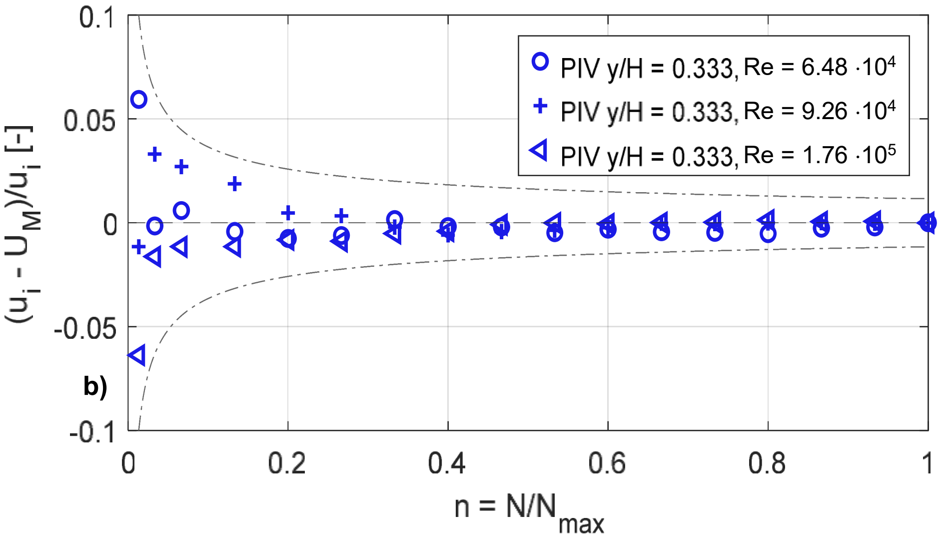

Figure 5: Convergence of ensemble-averaged mean velocity as normalized differences to the long-term mean $U_{M,max}$ over number of successive vector fields N_{max}, sampled at y/H = 0.333 for PIV and ADCP-based velocity data.

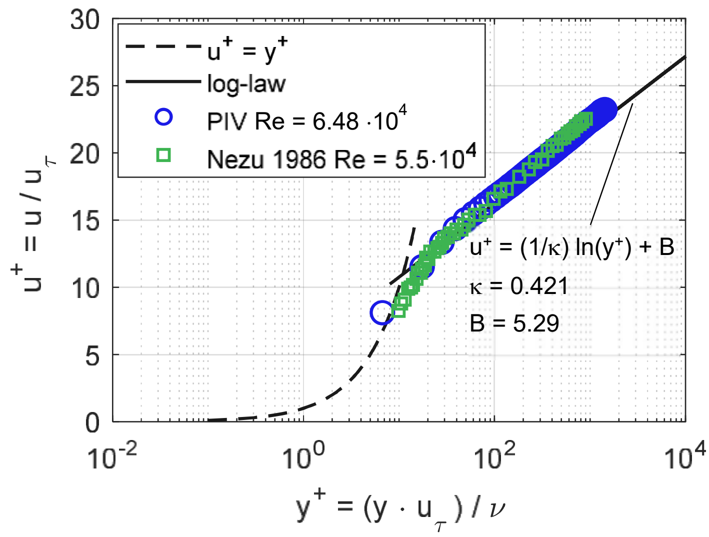

Figure 6: Normalized mean velocity $u^+ = (u / u_\tau)$ against dimensionless wall distance $y^+ = (y \cdot u_\tau) / \nu$ with friction velocity $u_\tau \cong 5.4$ mm/s estimated with the "Clauser method" (Clauser 1956).

4 Results and discussion

Preliminary results are presented in terms of mean velocity data from 2D2C-PIV and ADCP, which are shown in Fig. 7 and Fig. 8 for all 6 investigated Reynolds number cases including error bars indicating the 95 % confidence interval for PIV and ADCP results, respectively. In case of PIV- and ADCP based results, velocities are calculated as the ensemble mean of both in-plane components u_X and u_Y.

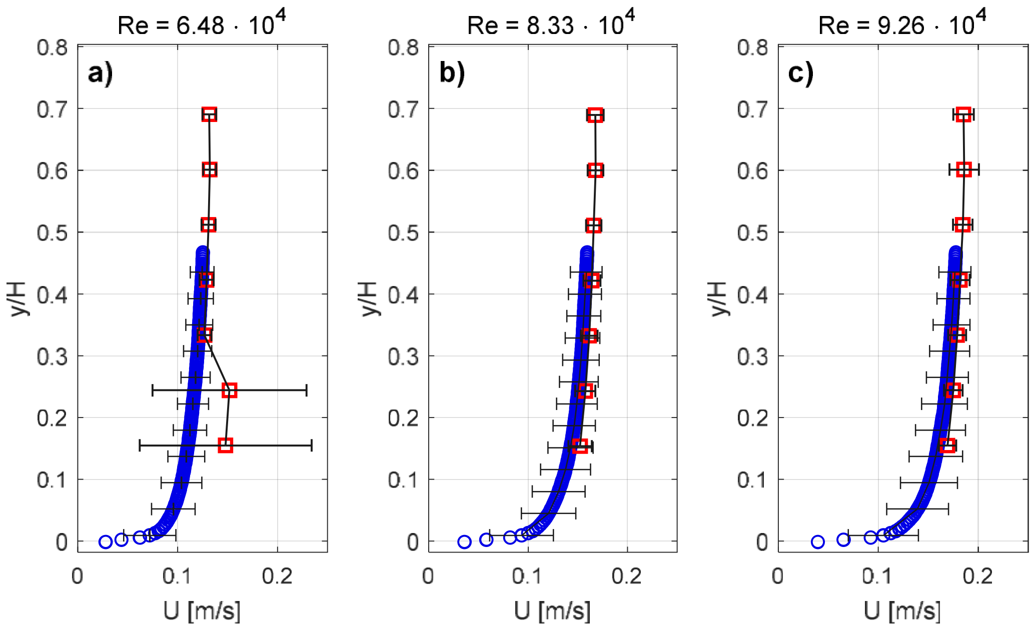

Figure 7: Ensemble averaged mean velocity data from PIV (blue circles) and ADCP (red squares), error bars indicating the 95 % confidence interval ($\pm$ 1.96 $\cdot$ σ_U) for PIV and ADCP results, respectively. Uncertainty bars for PIV and ADCP are partially covered by the markers, with a maximum relative uncertainty of the mean of 0.5 % for PIV-based and 0.25 % for ADCP-based velocity results.

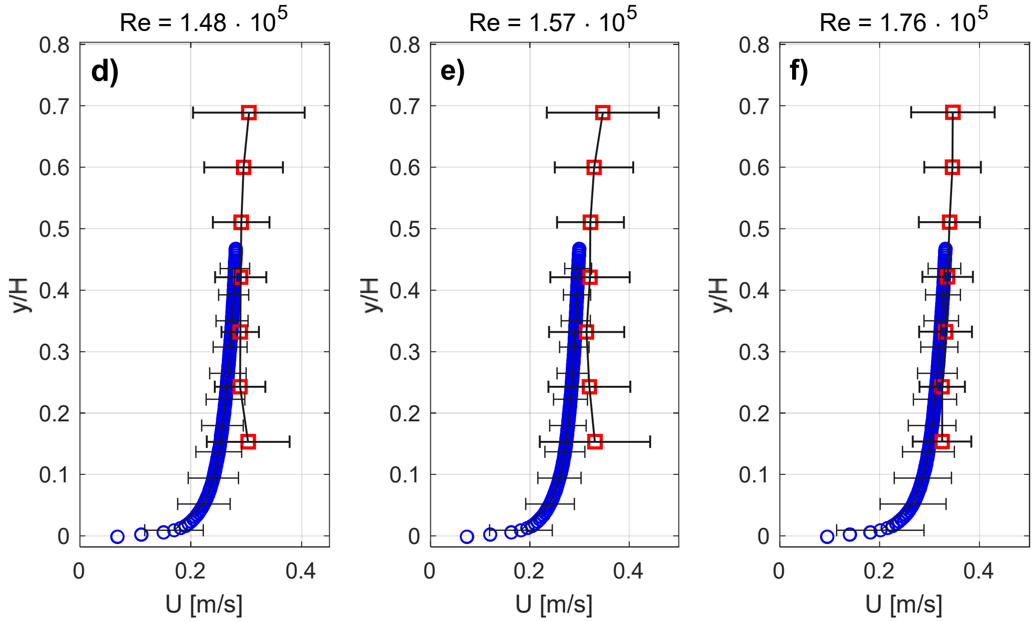

Figure 8: Ensemble averaged mean velocity data from PIV (blue circles) and ADCP (red squares), error bars indicating the 95 % confidence interval ($\pm$ 1.96 $\cdot$ σ_U) for PIV and ADCP results, respectively. Uncertainty bars for PIV and ADCP are partially covered by the markers, with a maximum relative uncertainty of the mean of 0.5 % for PIV-based and 0.25 % for ADCP-based velocity results.

The averaged velocity data show reasonable agreement, particularly for higher Reynolds numbers in the intermediate range. However, a deviation to 2D2C - PIV reference data is clearly observable, especially for near-wall data, see Fig. 7 a). Since we did not use any empirical extrapolation for mean velocity data in the lower and upper probe region, e.g. the channel ground region below y/H = 0.15, and the upper probe region above y/H = 0.423, relative deviations of mean values of up to 32 % are still present. Moreover PIV-based mean velocity data is also compared against Laser Doppler Anemometry (LDA) data of Nezu (Nezu and Rodi 1986), see Fig. 6 for the Re = 6.48 $\cdot$ 10^4 case. Minor deviations between ADCP and PIV measurements are observed in Fig. 7 and Fig. 8, particularly at low flow (subplot a)) and moderate-to-high flow cases (subplots d) and e)). In the lowest flow condition, the two near-bed ADCP bins deviate from the expected boundary layer trend, likely due to weak Doppler signals, blanking distance limitations, and low signal-to-noise ratio. In subplots d) and e), slight overestimations appear in the upper profile, which can be attributed to side-lobe interference and vertical averaging effects. These deviations occur in known ADCP uncertainty regimes and remain within reported confidence intervals, while the overall velocity profile shapes agree across all cases. A further pulsatile flow behavior of the channel was observed during the previously described measurements, mainly generated based on minor control deviations of the pump speed drive. Despite turbulent structures, this is considered to be a promoting factor which leads to higher velocity standard deviations, mentioned before.

The absolute and relative deviation between PIV- and ADCP-based results is also listed in Table 3 for all available ADCP data points equivalent to PIV data along the depth coordinate in terms of the root mean squared error (RSME), respectively.

Table 3: Root mean square error (RMSE) as absolute and relative deviation of PIV and ADCP time averaged mean velocity data for all ADCP data points (see. Fig. 7 and Fig. 8).

case		C1		C2		C3		C4		C5		C6	
y/h	y	ε	$\frac{\varepsilon}{\lvert U_{PIV}\rvert}$	ε	$\frac{\varepsilon}{\lvert U_{PIV}\rvert}$	ε	$\frac{\varepsilon}{\lvert U_{PIV}\rvert}$	ε	$\frac{\varepsilon}{\lvert U_{PIV}\rvert}$	ε	$\frac{\varepsilon}{\lvert U_{PIV}\rvert}$	ε	$\frac{\varepsilon}{\lvert U_{PIV}\rvert}$
[-]	[mm]	[m/s]	[%]	[m/s]	[%]	[m/s]	[%]	[m/s]	[%]	[m/s]	[%]	[m/s]	[%]
0.155	86.7	0.035	32.03	0.009	6.46	0.009	5.91	0.046	18.02	0.054	19.59	0.022	7.43
0.244	136.7	0.033	28.34	0.007	4.69	0.007	4.37	0.023	8.60	0.033	11.73	0.010	3.32
0.333	186.7	0.006	4.81	0.007	4.29	0.006	3.70	0.015	5.64	0.021	7.30	0.009	2.80
0.423	236.7	0.005	3.85	0.006	3.88	0.006	3.21	0.011	3.82	0.023	7.68	0.006	1.92

5 Summary and Conclusion

In this contribution we presented results of comparative velocity measurements by means of 2D2C-PIV and ADCP based data acquired in an open water channel under steady clear water conditions at zero inclination. From these preliminary results we can conclude first that the mean velocity acquired via ADCP was slightly overestimated compared to PIV-based results for all flow rates between 1.92 - 32.03 %, and all depth ratios between y/H = 0.155 to y/H = 0.423, respectively. For the low Reynolds number cases of Re = $6.48 \cdot 10^4$ and below we apparently approached the lower detection limit of the ADCP, which was confirmed by additional evaluation of the signal-to-noise ratio. A peak ratio below 0.3 in this case led to an increased discard of ADCP samples and therefore to higher statistical uncertainty. The acoustic signal quality was mainly deteriorated here by acoustic interferences within the channel due to short measurement distances (distance sensor to fixed wall, see. Fig. 2). This effect is believed to be also enhanced by the low mean flow velocities of about 0.09 m/s present in the channel at low Reynolds numbers of Re = $6.48 \cdot 10^4$ and below. In these cases, the ADCP tends to increasingly bias velocity estimates as the wall distance to the channel ground decreases. It was not possible to resolve the wall boundary layer in this case with the ADCP sensor.

A further investigation with advanced ADCP device settings, namely a higher spatial resolution and additional 2D3D-PIV data acquired in stream- and spanwise open-channel cross-sections will support a perimeter of faulty influences on ADCP - based velocity estimates, especially in the near-wall area close to the channel ground, which is crucial to determine decisive factors contributing sediment transport under laboratory conditions as part of further studies.

Acknowledgements

Financial support by the German Research Foundation (DFG) in the program “Forschungsimpulse” within the project “KOENIG - *A calibrated and virtual multi-scale wave measurement laboratory to improve and supplement flow measurements: From basic research to industrial application*” under project number 528740160 is gratefully acknowledged.

Literature

Adrian, R. J. (1997): Dynamic ranges of velocity and spatial resolution of particle image velocimetry. *Meas. Sci. Technol.* 8 (12), S. 1393–1398.

Adrian, R. J., Westerweel, J. (2011): Particle image velocimetry. Cambridge Univ. Press (Cambridge aerospace series, 30).

Chanson, H., 2009: The hydraulics of open channel flow: An introduction. Basic principles, sediment motion, hydraulic modelling, design of hydraulic structures. 2nd edition, Amsterdam, Boston, Heidelberg: Elsevier Butterworth Heinemann.

Chow, V. T., 2009: Open-channel hydraulics. Caldwell, NJ: Blackburn Press.

Clauser, F. H., 1956: The Turbulent Boundary Layer. Advances in Applied Mechanics Volume 4, Bd. 4: Elsevier (Advances in Applied Mechanics), S. 1–51.

Keane, R. D., Adrian, R. J., 1990: Optimization of particle image velocimeters. Part I. Double pulsed systems. *Meas. Sci. Technol.* 1 (11), S. 1202–1215.

Kim, D.-S., Kang, B.-S. 2011: Investigation of near transducer errors in acoustic Doppler current profiler measurements using experimental and numerical method. Journal of the Korea Academia-Industrial cooperation Society 12 (2), S. 944–951.

Legleiter, C. J., Kinzel, P. J., 2021: Surface flow velocities from space: Particle Image Velocimetry of satellite video of a large, sediment-laden river. *Front. Water* 3, 652213.

Mueller, D. S., Abad, J. D., García, C. M., Gartner, J. W., García, M. H., Oberg, K. A., 2007: Errors in acoustic Doppler profiler velocity measurements caused by flow disturbance. *J. Hydraulic Eng.* 133 (12), S. 1411–1420.

Muste, M. K., Dongsu, G.- C., Juan A., 2010: Near-Transducer Errors in ADCP Measurements: Experimental Findings. *J. Hydraul. Eng.* 136 (5), pp. 275–289.

Nezu, I., Rodi, W., 1986: Open-channel Flow Measurements with a Laser Doppler Anemometer. *J. Hydraul. Eng.* 112 (5), S. 335–355.

Nones, M., Dolcetti, G., Przyborowski, Ł., Mrokowska, M., Conevski, S., Guerrero, M., 2022: Experimental methods and instrumentation in hydraulics. *Acta Geophys.* 70 (5), S. 2201–2203.

Nystrom, E. A.; Oberg, K. A., Rehmann, C. R. 2002: Measurement of Turbulence with Acoustic Doppler Current Profilers - Sources of Error and Laboratory Results. In: Tony L. Wahl, Clifford A. Pugh, K. A. Oberg und T. B. Vermeyen (Hg.): Hydraulic Measurements and Experimental Methods 2002. (HMEM) 2002. Estes Park, Colorado, United States, July 28-August 1, 2002. Reston, VA: ASCE, S. 1–10.

Nystrom, E. A., Rehmann, C. R., Oberg, K. A., 2007: Evaluation of Mean Velocity and Turbulence Measurements with ADCPs. *J. Hydraul. Eng.* 133 (12), S. 1310–1318.

Sciacchitano, A., Wieneke, B., 2016: PIV uncertainty propagation. *Meas. Sci. Technol.* 27 (8), S. 84006.

Simpson, M. R. 2001: Discharge Measurements Using a Broad-Band Acoustic Doppler Current Profiler. U.S. Geological Survey. Sacramento, California.

Tuhin, M. T. H., Mudersbach, C. 2025: Integrating Machine Learning with ADCP Data for Advanced Sediment Transport and Hydrodynamics Monitoring. EGU General Assembly 2025, Vienna, Austria, 27 Apr – 2 May 2025, EGU25-8296

Westerweel, J., Scarano, F., 2005: Universal outlier detection for PIV data. *Exp. in Fluids* 39 (6), S. 1096–1100.

Wieneke, B., 2015: PIV uncertainty quantification from correlation statistics. *Meas. Sci. Technol.* 26 (7), S. 74002.

GALA e.V., Karlsruhe, Germany, ISBN 978-3-9827594-0-1